



**HAL**  
open science

## High temperature oxidation resistance and microstructure of laser-shock peened Ti-Beta-21S

L. Lavisse, A. Kanjer, P. Berger, V. Optasanu, Cyril Gorny, Patrice Peyre, T. Montesin, M.C. Marco de Lucas

► **To cite this version:**

L. Lavisse, A. Kanjer, P. Berger, V. Optasanu, Cyril Gorny, et al.. High temperature oxidation resistance and microstructure of laser-shock peened Ti-Beta-21S. *Surface and Coatings Technology*, 2020, 403, pp.126368. 10.1016/j.surfcoat.2020.126368 . cea-02933755

**HAL Id: cea-02933755**

**<https://cea.hal.science/cea-02933755>**

Submitted on 10 Sep 2020

**HAL** is a multi-disciplinary open access archive for the deposit and dissemination of scientific research documents, whether they are published or not. The documents may come from teaching and research institutions in France or abroad, or from public or private research centers.

L'archive ouverte pluridisciplinaire **HAL**, est destinée au dépôt et à la diffusion de documents scientifiques de niveau recherche, publiés ou non, émanant des établissements d'enseignement et de recherche français ou étrangers, des laboratoires publics ou privés.

# High temperature oxidation resistance and microstructure of laser-shock peened Ti-Beta-21S

L. Lavissee<sup>a,\*</sup>, A. Kanjer<sup>a</sup>, P. Berger<sup>b</sup>, V. Optasanu<sup>a</sup>, C. Gorny<sup>c</sup>, P. Peyre<sup>c</sup>, T. Montesin<sup>a</sup>, M. C. Marco de Lucas<sup>a,\*</sup>

<sup>a</sup>Laboratoire Interdisciplinaire Carnot de Bourgogne, UMR 6303 CNRS-Université Bourgogne-Franche Comté, 9 Avenue A. Savary, BP 47 870, F-21078 Dijon Cedex, France

<sup>b</sup>Université Paris-Saclay, CEA, CNRS, NIMBE, 91191 Gif-sur-Yvette, France

<sup>c</sup>Laboratoire PIMM, Ensam CNRS Cnam - Arts et Métiers - Sciences et Technologies - Ensam, 151 Boulevard de l'Hôpital, 75013 Paris, France

---

## Abstract

Improving the high temperature (HT) resistance of titanium alloys is currently a technological challenge for extending their use in aerospace engines. Ti-Beta-21S is a metastable  $\beta$  titanium alloy specifically designed for high temperature applications up to 593 °C. We report the effect of a surface treatment by laser-shock peening (LSP) on the high temperature behavior of Ti-Beta-21S in order to increase further its maximum service temperature. The oxidation kinetics at 700 °C for duration up to 3000 h showed that the LSP treatment increases the oxidation resistance of Ti-Beta-21S. The effects of the LSP treatment on the alloy microstructure, its evolution at high temperature and the diffusion of light atmospheric elements (oxygen and nitrogen) are also reported.

*Keywords:* Mechanical surface treatments, metastable beta-titanium, high temperature oxidation, oxidation kinetics, oxygen diffusion

---

## 1. Introduction

Aviation is currently one of the fastest-growing sources of greenhouse gas emissions. This is a huge ecological challenge for aeronautics. In order to reduce pollutant emissions, aircrafts of the future require the development of components with improved lightness, efficiency and durability. The excellent combination of lightness and good physical and chemical properties makes titanium alloys very attractive in this context [1, 2]. They are especially found in compressor blades and discs and engine housings, as well as in structures. However, their use is still limited to temperatures below 550 °C because of their

---

\*Corresponding authors

Email addresses: luc.lavissee@u-bourgogne.fr (L. Lavissee), delucas@u-bourgogne.fr (M. C. Marco de Lucas)

low resistance to oxidation above this limit [3]. Implementing Ti alloy components which could resist to higher temperatures would provide a mass gain of approximately 50% compared to nickel-based superalloys currently in use above 550 °C. Extending the use of these alloys to the turboengines of the aircraft of the future would make titanium alloys even more attractive.

Mechanical surface treatments such as shot-peening (SP) or laser-shock peening (LSP) appear as possible technological solutions to extend the service temperature range of various metals [4, 5]. Those techniques are already used in the industry to improve some particular properties of metals at ambient temperature: mechanical (fatigue resistance) [6, 7], tribological (resistance to wear) [8, 9] and electrochemical (resistance to pitting) [10]. The beneficial effect of SP and LSP treatments on the high temperature (HT) oxidation resistance of pure titanium at 700 °C has been reported by Kanjer *et al.* [11, 12]. The reduction of both the mass gain and the diffusion length of oxygen in the Ti-  $\alpha$  matrix [12], which corresponds to the so-called  $\alpha$ -case, were remarkable in LSP treated samples. To the best of our knowledge, the possibility of using this kind of surface treatments to increase the maximum application temperature of metastable beta titanium alloys has not been studied. The improved high specific strength and cool formability of metastable  $\beta$ -titanium alloys are great assets in aeronautics applications.

The aim of this study is to investigate the effect of the LSP treatment on the high temperature oxidation resistance of a metastable  $\beta$ -titanium alloy, as well as on the microstructure and its evolution at high temperature.

The material used for this work was the Ti-Beta-21S alloy from TIMET (TIMETAL 21S), which has been specifically designed for improved oxidation resistance, elevated temperature strength, creep resistance and thermal stability [13–15]. Ti-Beta-21S is reported by TIMET as suitable for high temperature applications up to 593 °C.

The study of the oxidation kinetics of LSP treated plates at 700 °C in dry air during 3000 h showed higher oxidation resistance of LSP treated samples compared to the reference material. The structural characterization of LSP treated samples and the analysis of the spatial distribution of the main alloying elements (molybdenum and aluminum) and light atmospheric elements (oxygen and nitrogen) after exposure at high temperature were addressed to explain the improvement of the oxidation resistance. Electron Backscattering Diffraction (EBSD) and scanning electron microscopy coupled to electron microprobe (EDS) were used for this purpose. Moreover, ion beam microanalysis was used for mapping the distribution of light elements in the cross-section of oxidized samples. The diffusion of oxygen and the insertion of nitrogen under the oxide scale have been investigated in this way.

## 2. Experimental details

### 2.1. The material

The material used in this study was the Ti-Beta-21S metastable  $\beta$  titanium alloy (TIMET supplier). This alloy is used in aeronautics for its good mechanical

and chemical resistance up to 600 °C. Stabilized mainly in the metastable  $\beta$ -Ti phase, its chemical composition (in wt.%) is: Ti 78, Mo 15.13, Nb 2.65, Fe 0.26, Si 0.2, Al 3.45, C 0.013, O 0.13, N 0.02.

For LSP treatments, pieces of 25 x 50 mm<sup>2</sup> were cut from 1.8 mm thick cold-rolled strips produced by TIMET. High temperature oxidation experiments were made on samples of 10 x 10 x 1.8 mm<sup>3</sup>.

In order to facilitate the reading of the following results, the untreated samples will be designated here by the abbreviation US, while those treated by laser-shock peening will be called LSP. Untreated and laser treated samples oxidized 3000 h at 700 °C will be called US-3000h and LSP-3000h, respectively.

## *2.2. Surface mechanical treatments and HT oxidation experiments*

Laser-shock peening was performed at the PIMM laboratory of ENSAM Paris, using a GAIA HP laser source [4]. After coating the surface of the sample with an aluminum foil tape, the samples were placed in a water container. The water media was used to confine the plasma plume produced by the laser beam. The aluminum coating absorbs the thermal effects generated by the laser irradiation and the water media amplifies both the amplitude and the duration of the shock effect within the treated material. The wavelength of the laser beam was 532 nm and the diameter of the focal spot was 4 mm. The duration of the laser shots was 7 ns and the frequency 0.5 Hz. The deposited laser irradiance was 9.1 GW/cm<sup>2</sup>. The laser beam scanned the sample surface on snake-shaped parallel lines with a velocity of 1.1 mm/s. The area of the overlap between two successive shots was 30%. The two faces of the sample were treated successively.

The treated and untreated samples (LSP and US) were oxidized under synthetic dry air at 700 °C during 3000 h by using a SETNAG quartz tube furnace. The samples were extracted every 160 h, weighed to evaluate their mass gain, and replaced into the furnace. Under these conditions, the material was thus cooled to room temperature and then put back to the oven after each weighting. A purge was carried out before introduction of the oxidizing gas, to avoid any presence of water vapors.

## *2.3. Characterization techniques*

The surface topography of the samples was studied using a VEECO WYCO NT 9100 optical profilometer.

X-ray diffraction phase analysis was carried out by using a BRUKER D8-A25 DISCOVER diffractometer. A Cu anticathode was used with beam incidence fixed at 2°.

The chemical state of the samples before HT oxidation experiments was analyzed by XPS (PHI Versaprobe 5000). In order to clean the sample surface, the very first superficial layers of the material were removed by bombardment with a 5 keV argon ion beam (Ar<sup>+</sup>) for 1 min.

After LSP treatment and oxidation for different durations of exposure to HT, the samples were cross-sectioned, resin-embedded and mechanically polished up to 50 nm colloidal silica suspension. Cross-sections of US and LSP samples were

analyzed by SEM coupled to an electron microprobe in order to investigate the distribution of the alloying elements (Mo, Al, ...). Two microscopes coupled to energy-dispersive spectroscopy (EDS) probes were used here, a TESCAN VEGA 3 and a field-emission microscope JEOL JSM-7600F.

The grain orientation was analyzed by Electron Backscattering Diffraction (EBSD) using a TSL EDAX OIM X4M EBSD system coupled with a JEOL-7600F microscope. The working distance was 20 mm, the tension 20 kV, the magnification  $\times 70$  and the step of scanning 1  $\mu\text{m}$ . Cross-sections of US-3000h and LSP-3000h samples were prepared as follows for EBSD analysis. The specimens were embedded in a cold-cure resin with rapid polymerisation and small shrinkage. They were mechanically polished with P600 and P1200 grit SiC papers. Then they were mirror-finished and slightly chemically etched using a 70:30 mixture of a colloidal silica suspension and  $\text{H}_2\text{O}_2$  on a polishing cloth (Presi, Supra).

Ion beam microanalysis was mainly used for mapping the distribution of light elements (oxygen and nitrogen) in the cross-section of oxidized samples. The operating principle of these techniques is summarized in Figure S1 (Supplementary Material). The nuclear microprobe of CEA-Saclay was used for this study. Depending on the implemented technique, the experimental beam conditions were as follows:

- Proton Induced X-ray Emission (PIXE) and Proton Induced Gamma-Ray Emission (PIGE) spectra were recorded with a 3 MeV proton beam (spot size 4.5  $\mu\text{m}$   $\times$  3.5  $\mu\text{m}$ ) for Ti ( $\text{K}_\alpha$  and  $\text{K}_\beta$  lines) and  $^{27}\text{Al}$  (1013 keV line), respectively.
- Nuclear Reaction Analysis (NRA) and Deuteron Induced Gamma-Ray Emission (DIGE) spectra were recorded with a 1.9 MeV deuteron beam (spot size: 4.5  $\mu\text{m}$   $\times$  3.5  $\mu\text{m}$ ) for the reactions of  $^{14}\text{N}$  ( $^{14}\text{N}(\text{d},\text{p}_i)^{15}\text{N}$  and  $^{14}\text{N}(\text{d},\alpha_i)^{12}\text{C}$ ), and  $^{16}\text{O}$  (871 keV line), respectively.

### 3. Results

#### 3.1. Consequences of LSP treatments on the raw material

Figure 1 presents a 3D reconstruction of the surface topography of the US and LSP samples of Ti-Beta-21S before and after the LSP surface treatment. The roller marks are clearly visible on the US sample, whereas they have practically disappeared after the laser treatment. The total roughness,  $R_t$ , slightly decreased from 6.4  $\mu\text{m}$  for US sample to 6.2  $\mu\text{m}$  for LSP sample. The average roughness,  $R_a$ , remained unchanged and equal to 0.4  $\mu\text{m}$  for both US and LSP samples.

The hardness profiles along the thickness (Figure S2) were measured on the cross-section of samples before and after LSP treatment. The variation of hardness along the thickness was negligible for both kinds of samples, and the mean value was around 330 HV. The absence of strain hardening leads to the

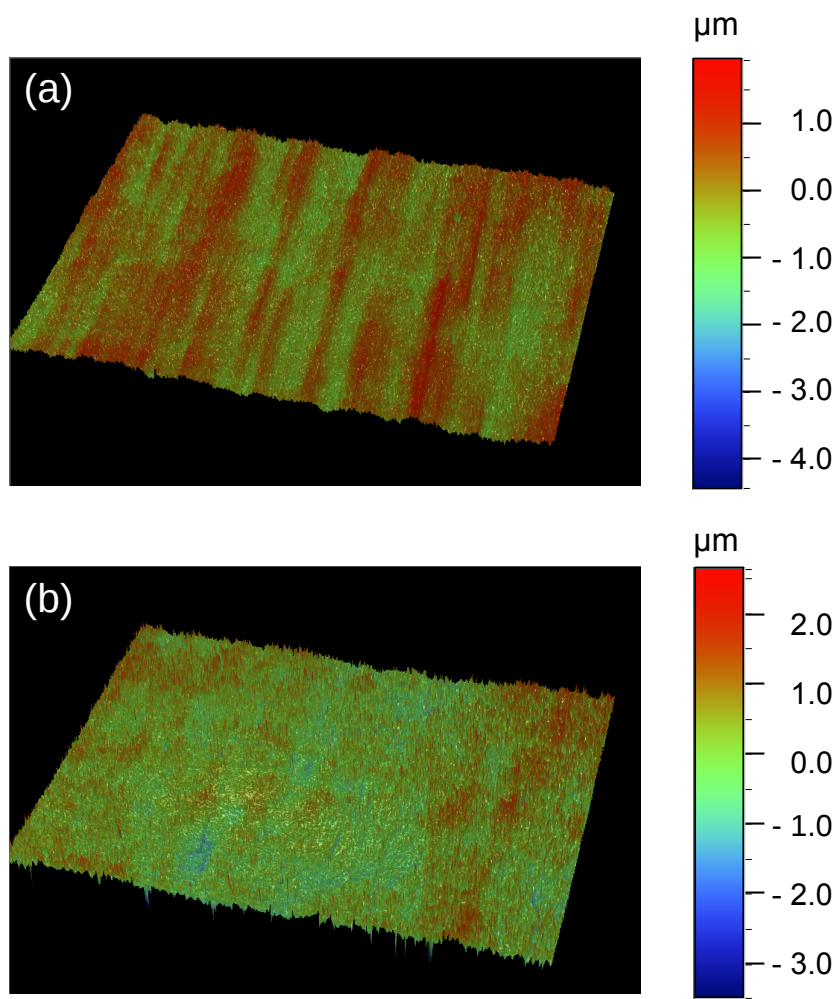


Figure 1: Surface optical profilometry of Ti-Beta-21S samples before (a) and after (b) the LSP treatment.

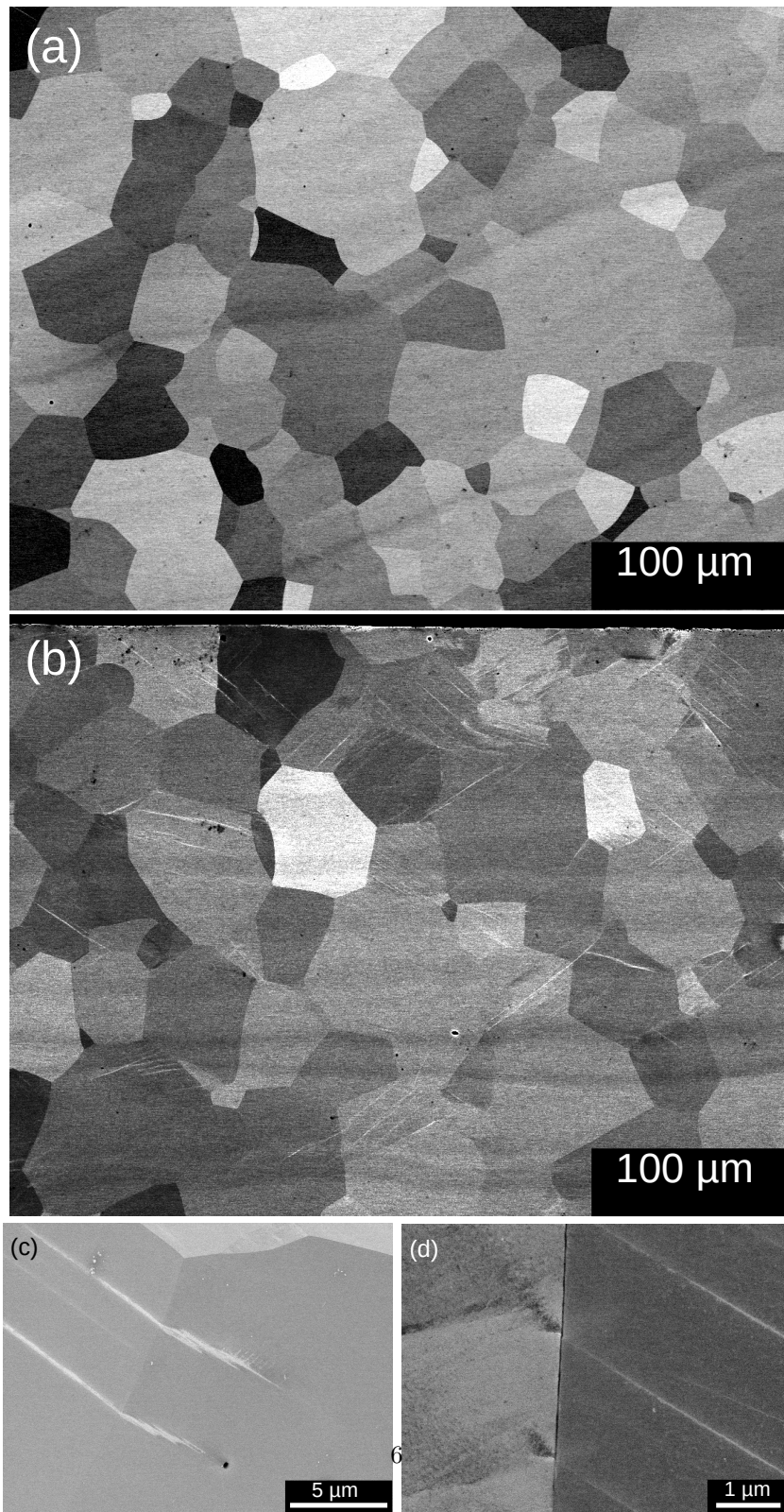


Figure 2: Cross-section SEM views of (a) US and (b) LSP samples. The surface of the cross-sectioned sample is at the top of both images. (c,d) High magnification views of the grain boundaries taken in the cross section of the LSP sample.

conclusion that the LSP treatment does not induce plastic deformation. The same result was obtained for the LSP treatment of pure  $\alpha$ -Ti [12].

The cross-sections of US and LSP samples were observed by SEM in back-scattering electrons mode (BSE) (Figure 2). The size distribution and the shape of the grains are similar for both US and LSP samples. However, only the images of LSP samples show in many areas a network of parallel straight lines (bright lines in Figure 2b) which cross the grains and which can extend into neighboring grains. High magnification views given in Figures 2c and 2d show these bright lines near the grain boundaries. The in-depth hardness profile has shown that the plastic deformation of the treated samples is negligible, so these lines cannot be explained as dislocations induced by the LSP treatment. Similar lines were also observed in the cross-section SEM images of LSP treated pure  $\alpha$ -Ti [12], and they were assigned to mainly compressive twins.

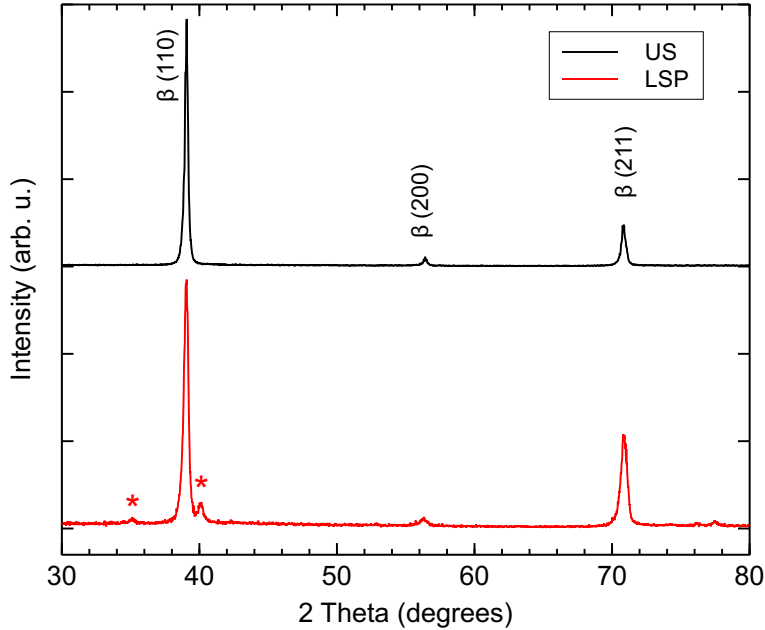


Figure 3: Grazing incidence X-ray diffraction patterns (incidence angle:  $2^\circ$ ) of untreated (US) and LSP treated samples. The peaks assigned to the  $\beta$ -Ti phase (ICSD: 0773482) are indicated. The intensity has been normalized to that of the  $\beta$ -Ti(100) reflection. The peaks tagged by stars (\*) have been tentatively assigned to the martensitic  $\alpha''$ -Ti phase.

Figure 3 displays the XRD patterns obtained with the beam incidence fixed at  $2^\circ$  for untreated and laser treated samples. The depth of the analyzed area was estimated around  $1 \mu\text{m}$ . The patterns of untreated samples show only the peaks of the  $\beta$ -Ti phase (ICSD: 0773482). For laser treated samples, the same diffraction peaks of the  $\beta$ -Ti phase are observed, but their absolute intensity is

smaller, and they are slightly broader. These effects can be mainly attributed to the disorder induced by the treatment and/or a refinement of crystallites on the surface. Nonetheless, the relative intensity between matching peaks of the  $\beta$ -Ti phase is quite similar in the patterns of both samples. This means that the laser treatment does not result in a different texturing than that produced after rolling.

The XRD patterns of LSP samples display also two additional small peaks at  $35.1$  and  $40.1^\circ$ , which reveal the presence of a second phase formed as a consequence of the LSP treatment. The position of these peaks is close to that given in ref. [16] for the  $\alpha$ -Ti phase formed in Ti-Beta-21S by oxidation at  $650^\circ\text{C}$  during 50 h. However, the heating induced by the LSP treatment is too low to induce the  $\beta \rightarrow \alpha$  phase transition. These small peaks at  $35.1$  and  $40.1^\circ$  could correspond to the martensitic  $\alpha''$ -Ti phase which in general can be formed by deformation of  $\beta$ -Ti at room temperature [17–20]. Here, the formation of  $\alpha''$ -Ti would be induced by the recoiled pressure of the laser-shock wave.

In order to investigate the chemical composition at the extreme surface, XPS analyses were conducted for US and LSP samples. The results are shown in Figure 4 in the spectral ranges corresponding to the XPS lines Ti2p, Al2p and O1s. The spectra showing the XPS lines Mo3d, Mo3p and Nb3d are given in Figure S3 (Supplementary Material).

For the US sample, Figure 4a displays the characteristic spectrum of metallic titanium which shows the Ti2p<sub>3/2</sub> and Ti2p<sub>1/2</sub> lines at 453.7 and 459.8 eV, respectively [21]. The slight broadening of both peaks towards higher binding energies observed for LSP samples can be interpreted as due to a slight oxidation of the surface. As a reference, Ti<sup>4+</sup>2p<sub>3/2</sub> line is given at 458.5 eV and Ti<sup>4+</sup>2p<sub>1/2</sub> at 464.2 eV for TiO<sub>2</sub> [21].

For the Al2p line (Figure 4b), the main peak corresponds for both samples to metallic aluminum, Al<sup>0</sup>2p<sub>3/2</sub> at 72.7 eV [22]. For the LSP sample, a small component at about 75.2 eV can be attributed to Al<sup>3+</sup>2p<sub>3/2</sub> [22]. The XPS lines of molybdenum and niobium (Figure S3) suggest also a slight surface oxidation of the LSP sample.

As regards oxygen, the shape of the O1s line (Figure 4c) is slightly different for US and LSP samples. The O1s line corresponding to O-Ti bonds has been reported at about 530 eV, while that corresponding to O-Al bonds is at about 532 eV and that for O-Ti bonds at about 530 eV [22, 23]. Compared to the US sample, the relative intensity of the contribution associated to Ti-O bonds is higher in the spectrum of LSP samples. This shows that the surface oxidation of LSP samples is slightly higher compared to US samples.

### 3.2. Kinetics of the high temperature oxidation

Figure 5 shows the variation of the mass gain reported to the surface of the sample,  $\Delta m/S$ , in US and LSP samples for non-isothermal oxidation at  $700^\circ\text{C}$ . The mass gain of LSP treated samples after exposure to high temperature for 3000 h is about 2.5 times smaller for laser-shock treated samples compared to untreated ones. So, the mass gain is about 60% smaller for laser-shock treated

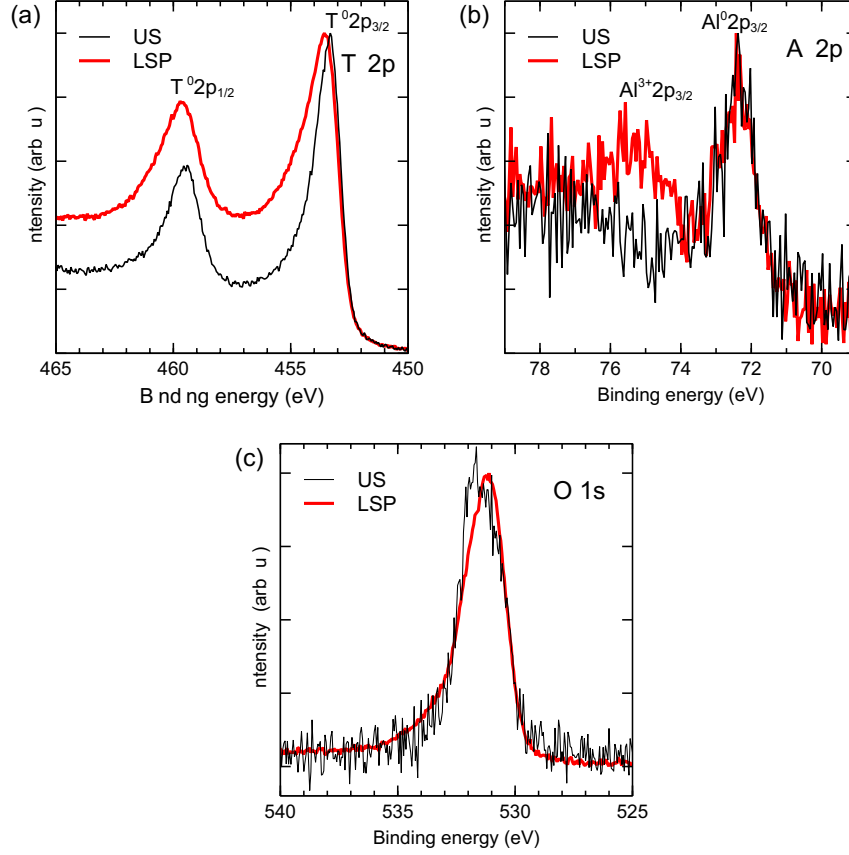


Figure 4: XPS spectra of untreated (US) and laser treated samples (LSP) in the spectral ranges corresponding to the following XPS lines: (a) Ti2p, (b) Al2p and (c) O1s.

Ti-Beta-21S. This clearly demonstrates the benefits of the LSP treatment to increase the oxidation resistance of Ti-Beta-21S at 700 °C.

The analysis of the oxidation kinetics was done on the basis of the most-general expression of parabolic kinetics as proposed by Monceau and Pieraggi [24]:

$$t = a_0 + a_1(\Delta m/S) + a_2(\Delta m/S)^2 \quad (1)$$

where  $t$  is the time,  $\Delta m$  the mass intake,  $S$  the sample surface, and  $a_i$  ( $i = 0, 1, 2$ ) the fitting coefficients. The reciprocal of  $a_2$  is equal to the parabolic rate constant,  $k_p$ , which describes the effect of the diffusion processes on the mass intake. A parabolic law is associated to an effective protection of the metal against the oxidation provided by the oxidation scale, which grows with a

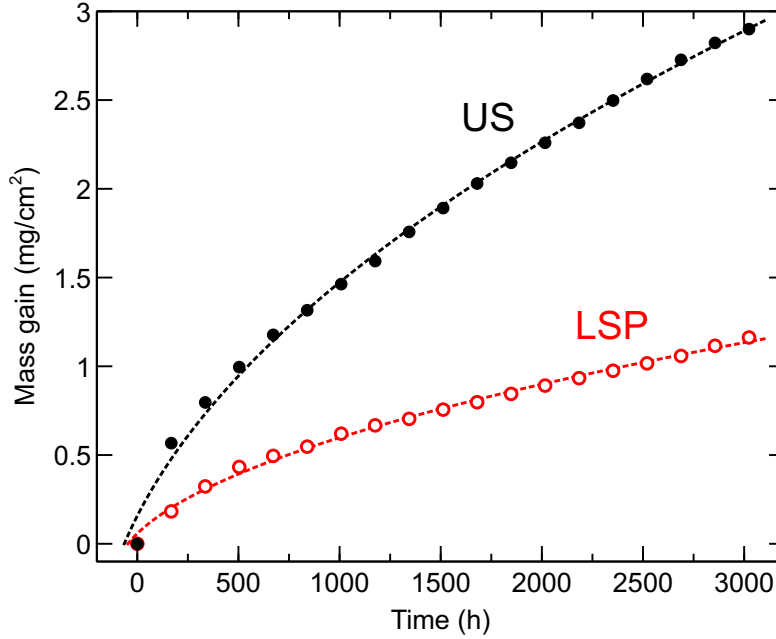


Figure 5: Mass gain curves of US and LSP samples during oxidation at 700 °C under synthetic dry air. Dotted lines correspond to the fitting of the experimental data to equation 1 with the parameters given in Table 1.

continuing decreasing rate [25]. The reciprocal of  $a_1$  is the linear rate constant,  $k_l$ , which together with the coefficient  $a_0$  depends on the initial thickness of the oxide and the oxidation mechanisms involved in a transient period.

The experimental data were fitted to equation (1) in the 0-3000 h range. The fitting parameters are given in Table 1, together with the corresponding linear and the parabolic rate constants. The linear rate constant,  $k_l$ , is almost 2 times higher for the untreated Ti-Beta-21S compared to the laser treated alloy. The parabolic rate constant,  $k_p$ , is about 7 times higher for the US sample than for the LSP one.

### 3.3. Effects of high temperature exposure on the microstructure and the diffusion of alloying and light atmospheric elements

Figure 6 shows the XRD patterns of US and LSP samples oxidized for 3000 h at 700 °C in dry air. The main phase observed for both samples is TiO<sub>2</sub>-Rutile. A small contribution of Al<sub>2</sub>O<sub>3</sub>-corundum can also be identified, mainly for the US-3000h sample. This is in agreement with the results reported by Wallace et al. [26] and by Behera et al. [16] showing the formation of an alumina layer on the top of the rutile scale. Stringer et al. [27] also showed the formation of a small amount of molybdenum oxide in the scale in the high temperature oxidation of

Sample	$a_0$ ( $h^{-1}$ )	$a_1$ ( $h.g^{-1}.cm^2$ )	$a_2$ ( $h.g^{-2}.cm^4$ )	$k_l$ ( $s^{-1}.g.cm^{-2}$ )	$k_p$ ( $s^{-1}.g^2.cm^{-4}$ )
US	-64.3	371.7	238.3	$7.47 \times 10^{-10}$	$1.17 \times 10^{-12}$
LSP	-46.5	703.0	1751.1	$3.9 \times 10^{-10}$	$1.59 \times 10^{-13}$

Table 1: Results of fitting the experimental oxidation curves (Figure 5) to a complete parabola (eq. 1). The linear rate constant,  $k_l$  is the reciprocal of  $a_1$ , and the parabolic rate constant,  $k_p$  is the reciprocal of  $a_2$ .

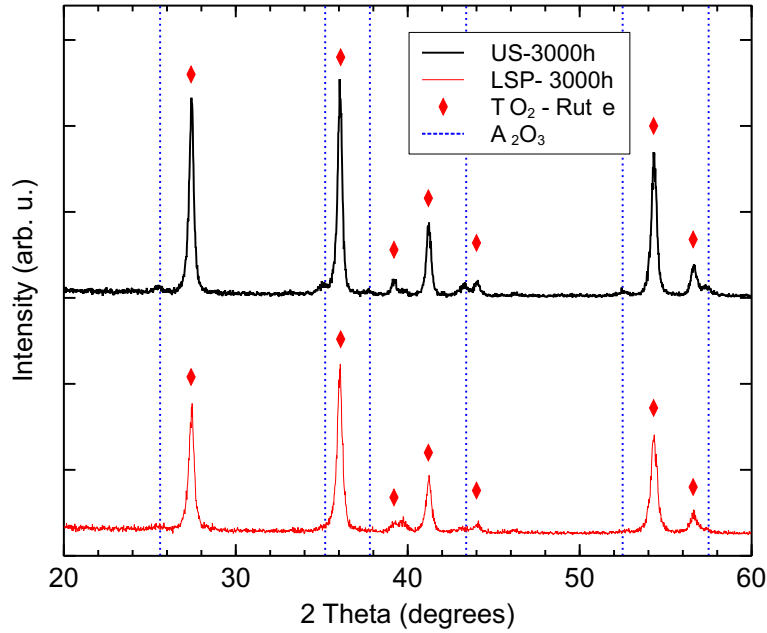


Figure 6: Grazing incidence XRD patterns of untreated (US) and laser treated samples (LSP) after oxidation at 700 °C during 3000 h. ICDS number of the compounds and phases identified in the pattern: TiO<sub>2</sub>-Rutile: 070-7347, Al<sub>2</sub>O<sub>3</sub> (corundum): 070-5679.

a Ti-15% Mo alloy. However, the volatilization process of molybdenum oxide, MoO<sub>3</sub>, at high temperature is well known [28]. Here, no diffraction peaks of MoO<sub>3</sub> or mixed oxides could be clearly identified.

Figure 7 displays cross-section maps of oxidized US-3000h and LSP-3000h samples showing the spatial distribution of  $\beta$ -Ti (in green) and  $\alpha$ -Ti (in red) phases obtained by EBSD study of both samples.

For the US-3000h sample, the  $\beta$ -Ti phase is found in about 60% of the cross-section image, while 40% corresponds to  $\alpha$ -Ti phase. For the LSP-3000h sample, the percentage of  $\beta$ -Ti phase is higher, about 68%, while 32% corresponds to  $\alpha$ -Ti phase. The ratio  $\beta$ -Ti/ $\alpha$ -Ti increases from 1.5 for US-3000 to 2.1 for LSP-

3000h, which shows that the LSP treatment acts to inhibit the  $\beta \rightarrow \alpha$  phase transition.

Moreover, the distribution of the  $\alpha$ -Ti phase is different in both samples. For the untreated sample, the  $\alpha$ -Ti phase is mainly found in the grain boundaries which are broadened. For the LSP-3000h sample, the  $\alpha$ -Ti is not mainly formed in the grain boundaries, but inside the grains. For both samples, the percentage of  $\alpha$ -Ti phase is higher near the surface (on top of both images in Figure 7). In a range going from the surface to 30  $\mu\text{m}$  in-depth, the percentage of  $\alpha$ -Ti phase increases to about 53% for the SP-3000h sample, while it is about 39% for the LSP-3000h sample.

In order to investigate the segregation of the alloying elements due to high temperature exposure, SEM observations were coupled to EDS mapping of different elements. Cross-section SEM views and EDS maps showing the spatial distribution of Ti, Al and Mo are given in Figure 8 for US and LSP samples.

After 3000 h at 700 °C, the thickness of the oxide scale has increased in both samples, but it is clearly thinner in the LSP sample than in the US one. For the US sample the thickness of the oxide scale is not homogeneous, it can vary from about 10 to 35  $\mu\text{m}$  thick. In these latter zones the scale is stratified and then provides little protection against oxidation. For the LSP sample, the oxide scale is quite homogeneous and only about 6  $\mu\text{m}$  thick. It can provide an effective protection to the metal. Aluminum is clearly observed in a layer at the extreme outer surface of US and LSP samples. This agrees with XRD results, and supports the existence of a thin layer of alumina on top of the scale [16, 26]. Underneath the oxide scale, Figure 8 shows also a clear difference in the grain boundaries, which are quite broader for the US sample (about 2-5  $\mu\text{m}$  thick) than for the LSP sample (about 1-2  $\mu\text{m}$  thick). The spatial resolution of EDS is barely sufficient for the analysis of the grain boundaries in LSP-3000h, but it is suitable for their analysis in US-3000h. The segregation between  $\alpha$ - and  $\beta$ -stabilizing elements in the metal is clearly observed. At the grain boundaries, the concentration of aluminum is higher, whereas that of molybdenum is lower. This segregation of  $\alpha$ - and  $\beta$ -stabilizing elements is also observed inside the grains.

The spatial distribution of light elements (oxygen and nitrogen) in the cross-section of these samples was also studied by EDS, but the overlap between the  $K_\alpha$  lines of nitrogen and oxygen with the  $L_\alpha$  and  $K_1$  lines titanium penalizes the accuracy of the results. Figure S4 (Supplementary Material) displays the concentration profiles obtained for both metallic and non-metallic elements way.

To overcome this problem, ion-beam analysis techniques were used here to study the distribution of light elements in oxidized samples. Figure 9 displays cross-section maps showing the spatial distribution of light elements (O and N) over 200 x 200  $\mu\text{m}$ , as well as the distribution of metallic elements (Ti, Al and Mo) over 300 x 300  $\mu\text{m}$ .

The spatial distribution of oxygen clearly shows the oxidation scale at the top of the images for both US-3000h and LSP-3000h samples, but its thickness is quite bigger for the untreated sample. Moreover, the spatial distribution of titanium shows the stratification of the oxidation layer in some areas (on the left

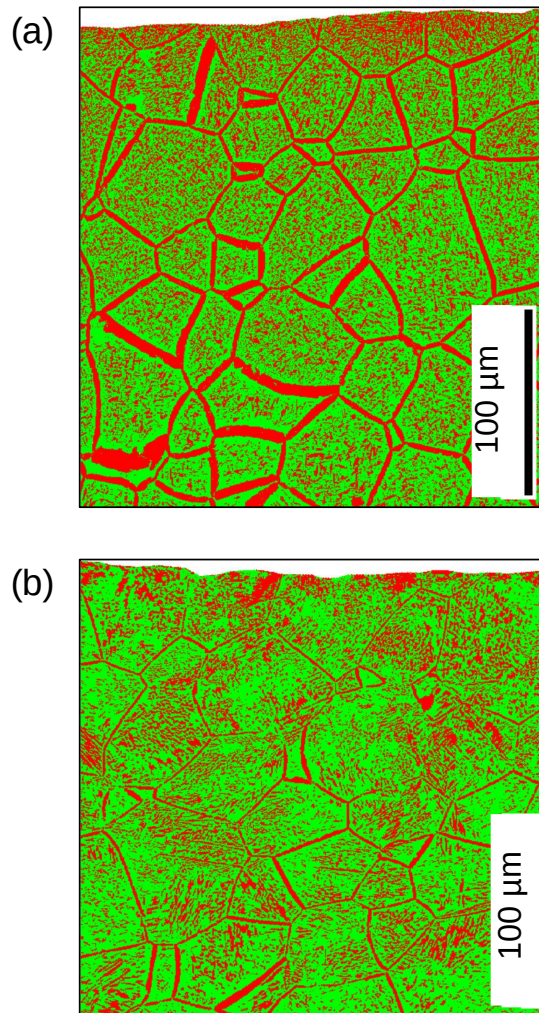


Figure 7: EBSD results showing the spatial distribution of  $\beta$ -Ti (in green) and  $\alpha$ -Ti (in red) phases in the cross section of (a) US-3000h and (b) LSP-3000h samples. The surface of the cross-sectioned sample is at the top of both images.

in Figure 9). Between two sublayers of the oxidation scale the Al-maps shows a higher concentration of aluminum, which reveals the formation of alumine  $\text{Al}_2\text{O}_3$  on the top of the sublayers. A similar effect is not observed for molybdenum.

Under the oxide scale, the spatial distribution of Ti shows in Figure 9 the grain boundaries in the metal, as it was previously observed in EDS maps (Figure 8). Unfortunately, the low signal-to-noise ratio in aluminum and molybdenum maps prevents observing the segregation of these elements in the grain boundaries.

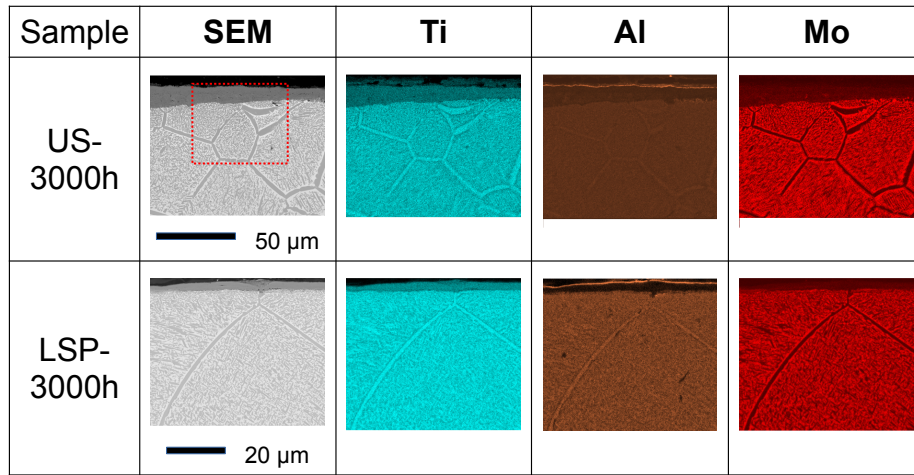


Figure 8: Cross-section SEM views of US-3000h and LSP-3000h samples recorded in back-scattering electrons (BSE) configuration, and elemental EDS maps corresponding to the spatial distribution of titanium, aluminum and molybdenum. The surface of the cross-sectioned sample is at the top of the images. A higher magnification was used for the observations of the LSP-3000h sample. For easier comparison, a dotted red rectangle of  $60 \times 50 \mu\text{m}^2$  displays in the SEM image of US-3000h sample the size of the area analyzed for the LSP-3000h sample.

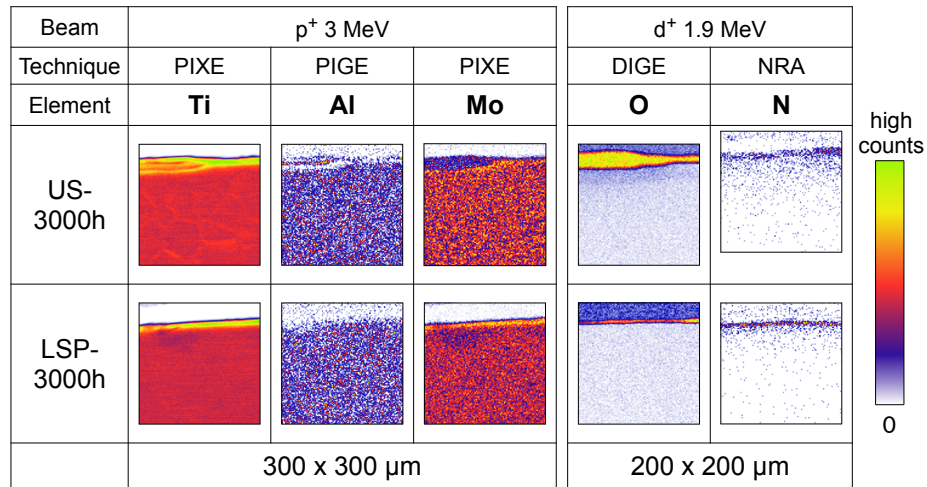


Figure 9: Spatial distribution of different elements (Ti, Al, Mo, O and N) in the cross-section of US-3000h and LSP-3000h samples obtained by different ion-beam microanalysis techniques (see section 2.3). The surface of the cross-sectioned sample is at the top of the images. The characteristics of the ion beam and the IBA technique used for detecting each element are also indicated.

As regards the distribution of light elements under the oxide scale, Figure 9 shows the diffusion of oxygen in the metal, which seems to be smaller in LSP treated samples than in untreated samples. To better study this effect, the variation in depth of the DIGE signal of oxygen has been plotted in Figure 10 by using the experimental data of Figure 9 for oxygen. For both US and LSP samples, the highest signal corresponds to the oxide scale. However, the low thickness of the scale (similar to the step in IBA maps) for the LSP-3000h prevents obtaining the high intensity measured for the US-3000h sample. Under the oxide scale, the signal of oxygen drastically falls down for both samples, but there are significant differences between both samples. For the treated sample, the signal of oxygen is very low and nearly constant in the analyzed range. For the untreated sample, the oxygen signal far deep from the oxide is slightly higher than for the treated sample, moreover, it is higher in a 20  $\mu\text{m}$  thick strip under the oxide scale. It is worth to note the large thickness and the stratification of the oxide above this area.

The atomic concentration of oxygen as a function of the oxygen signal has been calculated by using the signal of the oxide scale as a reference corresponding to  $\text{TiO}_2$ . The difference in the slowing of the incident beam of deuterons as a function of the  $\text{TiO}_x$  stoichiometry was addressed by using the Pyrole software [29]. Further details are given as Supplementary Material (Figure S5). For the US-3000h sample, the stoichiometry is about  $\text{TiO}_{0.092}$  (8.4 at.% O) in a 20  $\mu\text{m}$  thick strip under the oxide scale, but it decreases to  $\text{TiO}_{0.012}$  (1.2 at.% O) 150  $\mu\text{m}$  far in depth from the oxide scale. For the LSP-3000h sample, the concentration of oxygen in the metal is smaller compared to US-300. It is negligible far in-depth in the metal, and it slightly increases up to about 0.5 at.% just under the oxide scale.

IBA experiments revealed the presence of nitrogen in the oxidized samples (Figure 9). Nitrogen was clearly detected in both untreated and treated samples under the oxide scale, but its distribution is different. For the laser treated sample, nitrogen is located in a thin layer just under the oxide scale, while it spreads more in the metal for the untreated sample without forming a continuous layer under the oxide scale. The narrow in-depth spatial distribution of nitrogen and the low intensity of the NRA signal do not allow to extract a in-depth profile as done for the oxygen.

#### 4. Discussion

The study of the HT oxidation resistance of untreated and laser treated Ti-Beta-21S at 700 °C during 3000 h has shown the beneficial effects of the laser treatment. They can be summarized as follows:

- The mass gain is reduced about 60% for non-isothermal oxidation during 3000 h.
- The oxidation scale is homogeneous and unstratified.

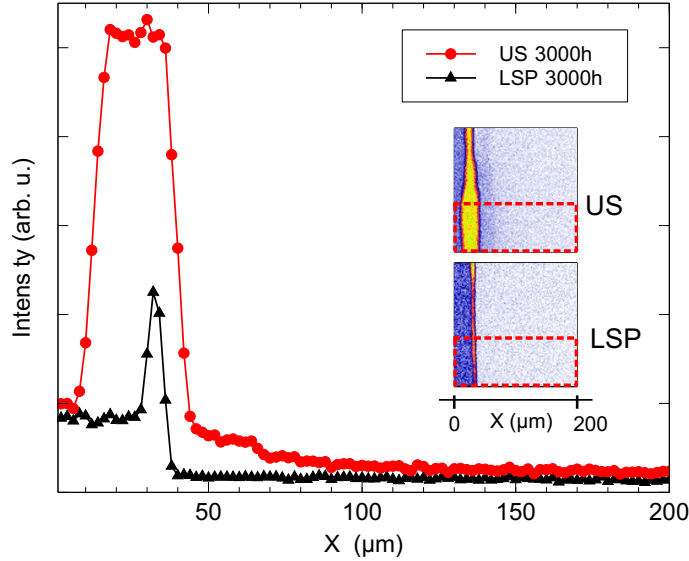


Figure 10: Oxygen depth profile in the US-3000h and LSP-3000h samples. The intensity of the oxygen signal in the DIGE maps of Figure 9 was summed at each depth  $X$  in the  $40 \mu\text{m}$  large rectangles (red delimited domains in the image) to increase the S/N ratio, and plotted as a function of depth ( $X$ ).

- The in-depth diffusion of oxygen in the alloy under the oxide scale is also reduced.
- The insertion of nitrogen in a thin and continuous layer at the interface between the oxide scale and the metal.
- The  $\beta \rightarrow \alpha$  phase transition at high temperature is partially inhibited, even  $200 \mu\text{m}$  under the sample surface.

The reasons explaining these changes in the HT oxidation behavior of laser treated Ti-Beta-21S should be sought in the changes induced by the laser treatment in the sample surface and also in-depth in the alloy. The changes at the sample surface concern mainly the topography of the sample. The LSP treatment flattens the roller marks due to the lamination process of Ti-Beta-21S and slightly reduces the total roughness. It induces also a slight oxidation of the surface. The induced hardening is negligible. The surface modified in this way can promote the growth at high temperature of a more compact oxide scale compared to untreated samples. However, the changes induced in the surface cannot explain all the effects summarized above.

The in-depth effects induced by the LSP treatment must be related to the propagation of the shock-wave in the sample. The analysis of laser treated samples has shown a partial transformation of the  $\beta$ -Ti phase into the martensitic

$\alpha''$ -Ti phase. We have related this effect with the observation in SEM cross-section observations of laser treated samples of a network of lines crossing the grains of  $\beta$ -Ti. Taking into account that the hardening induced by the treatment is negligible, these lines cannot be assigned to dislocations. The experimental conditions used here for the laser treatment lead to the formation of a plasma over the surface sample which extends over about ten microseconds for each shot [10]. This plasma induces a pressure smaller than the yield strength of Ti-Beta-21S. The shock-wave propagates in-depth in the sample at around 5000 m/s and it can be reflected on the bottom sample surface 1.8 mm below. The interference between incident and reflected waves can induce shearing strains which can promote twinning. The lines observed in the cross section of LSP samples can be due to this effect. This explanation is supported by the presence of peaks assigned to the  $\alpha''$ -Ti phase in the XRD pattern recorded for LSP samples before the oxidation experiments.

Different works [20, 30–32] have studied the stress-induced martensitic transition (SIMT) of  $\beta$ -Ti alloys during deformation at room temperature. They have shown that in metastable  $\beta$ -Ti alloys with a low molybdenum equivalency (about 8.1 wt%), SIMT is the primary deformation mode. The start of yielding can correspond to the triggering of SIMT eventually followed by dislocation slip at a higher stress, but both effects can also operate simultaneously [30].  $\alpha''$ -Ti plates have been observed by SEM and TEM [30].  $\alpha''$ -Ti is mechanically twinned, and its substructure can influence the twinning in the  $\beta$ -Ti phase.

For Ti-Beta-21S, the molybdenum equivalency about 13 wt% is quite higher than the stability limit  $\alpha$ -Ti+ $\beta$ -Ti /  $\beta$ -Ti about 10 wt%. The aluminum equivalency is low, about 5 wt%. The shock-laser treatment induces fast mechanical stress with very low heating. In these conditions, SIMT can appear without dislocation slip. The presence of  $\alpha''$ -Ti could modify the  $\beta$ -Ti  $\rightarrow$   $\alpha$ -Ti phase transition at high temperature by reducing the diffusion of alpha-stabilizing aluminum towards the grain boundaries where the  $\beta$ -Ti  $\rightarrow$   $\alpha$ -Ti transition is mainly observed in untreated Ti-Beta-21S.

Oxygen is also an alpha-stabilizing element. As regards its in-depth diffusion from the sample surface and its spatial distribution in the cross-section maps, the results do not show a significant increase of the concentration in oxygen at the grain boundaries of oxidized untreated (US) samples, where the  $\alpha$ -Ti phase is formed at high temperature. This suggests that the diffusion of oxygen does not occur preferentially following the grain boundaries, but it takes place in the grains. The in-depth diffusion of oxygen in the alloy is also reduced by the laser treatment. This could be explained by the insertion of nitrogen in a thin and continuous layer at the interface between the oxide scale and the metal shown by IBA experiments. This layer of nitrogen would reduce the diffusion of oxygen towards the metal. This effect has been previously reported for  $\alpha$ -Ti [12].

## 5. Conclusions

This work shows the beneficial effect of a laser-shock peening (LSP) treatment on the high temperature oxidation resistance of the metastable  $\beta$  titanium

alloy Ti-Beta-21S which has been studied for a long exposure time at 700 °C in dry air. After 3000 h, the mass gain in LSP treated samples is reduced by about 60% compared to untreated Ti-Beta-21S. The oxidation scale is thinner and more homogeneous for LSP treated samples compared to untreated specimens that present stratified oxide scales. In both cases, the oxidation layer is mainly composed of rutile with a thin layer of alumina on top of the scale. Below the oxide, we have detected the insertion of nitrogen in a narrow strip. The concentration of nitrogen is higher in laser treated samples.

The LSP treatment modifies the topography of the surface of the samples by flattening the roller marks. It also induces a slight oxidation of the surface while the induced hardening is negligible. Beyond the surface, the impact of the LSP treatment on the microstructure was revealed in SEM cross-section views by the apparition of a network of lines crossing the grains of laser treated samples. This effect was assigned to a partial transformation of the  $\beta$ -phase into the martensitic  $\alpha''$ -phase detected by XRD.

The analysis of oxidized untreated and laser treated samples under the oxidation scale has shown that the LSP treatment partially inhibits the  $\beta \rightarrow \alpha$  phase transition at the grain boundaries. It is mainly found for untreated samples together with the segregation of molybdenum and aluminum. For laser treated samples, the  $\alpha$ -phase is formed mainly inside the grains. The following explanation has been proposed based on the martensitic transformation induced by the laser treatment: at high temperature the  $\alpha''$  phase transforms into the  $\alpha$  which reduces the diffusion of aluminum towards the grain boundaries and of molybdenum towards the grains core.

The diffusion of oxygen in the metal is also smaller in laser treated samples. This is noteworthy to preserve the properties of Ti-Beta-21S under high temperature exposure. The compactness of the oxide scale and the insertion of nitrogen in a thin layer under the oxide scale, acting as a break to oxygen diffusion, could explain this behavior.

In summary, the surface treatment of Ti-Beta-21S alloy by laser-shock peening is a suitable method for extending its maximum application temperature in dry air.

## Acknowledgements

The authors thank O. Heintz, N. Geoffroy and F. Herbst from the ICB laboratory and M. Saint-Jean from the IUT Chalon sur Saône for their contribution to the experimental observations and analyses, and Prof. B. Domenichini for his expertise in the analysis of XPS results. This work has been supported by the EIPHI Graduate School (contract ANR-17-EURE-0002).

## References

- [1] J. C. Williams, E. A. Starke, Progress in structural materials for aerospace systems, *Acta Materialia* 51 (2003) 5775–5799.

- [2] K. Inagaki, T. Takechi, Y. Shirai, N. Ariyasu, Application and features of titanium for the aerospace industry, Technical Report, Nippon Steel and Sumitomo Metal 106 (2014) 22–27.
- [3] J. Stringer, The oxidation of titanium in oxygen at high temperatures, *Acta Metallurgica* 8 (1960) 758–766.
- [4] R. Fabbro, P. Peyre, L. Berthe, X. Scherpereel, Physics and applications of laser-shock processing, *Journal of Laser Applications* 10 (1998) 265–279.
- [5] L. Raceanu, V. Optasanu, T. Montesin, G. Montay, M. François, Shot-peening of pre-oxidized plates of zirconium: Influence of residual stress on oxidation, *Oxidation of Metals* 79 (2012) 135–145.
- [6] X. C. Zhang, Y. K. Zhang, J. Z. Lu, F. Z. Xuan, Z. D. Wang, S. Tu, Improvement of fatigue life of Ti–6Al–4V alloy by laser shock peening, *Materials Science and Engineering: A* 527 (2010) 3411–3415.
- [7] E. Maawad, Y. Sano, L. Wagner, H.-G. Brokmeier, C. Genzel, Investigation of laser shock peening effects on residual stress state and fatigue performance of titanium alloys, *Materials Science and Engineering: A* 536 (2012) 82–91.
- [8] S. A. Chamgordani, R. Miresmaeili, M. Aliofkhazraei, Improvement in tribological behavior of commercial pure titanium (CP-Ti) by surface mechanical attrition treatment (SMAT), *Tribology International* 119 (2018) 744–752.
- [9] M. Rajabi, R. Miresmaeili, M. Aliofkhazraei, Hardness and wear behavior of surface mechanical attrition treated titanium, *Materials Research Express* 6 (2019) 065003.
- [10] P. Peyre, X. Scherpereel, L. Berthe, C. Carboni, R. Fabbro, G. Béranger, C. Lemaitre, Surface modifications induced in 316L steel by laser peening and shot-peening. influence on pitting corrosion resistance, *Materials Science and Engineering: A* 280 (2000) 294–302.
- [11] A. Kanjer, V. Optasanu, L. Lavissee, M. C. Marco de Lucas, S. Dejardin, M. François, P. Berger, P. Peyre, C. Gorny, T. Montesin, Influence of mechanical surface treatment on high-temperature oxidation of pure titanium, *Oxidation of Metals* 88 (2017) 383–395.
- [12] A. Kanjer, L. Lavissee, V. Optasanu, P. Berger, C. Gorny, P. Peyre, F. Herbst, O. Heintz, N. Geoffroy, T. Montesin, M. C. Marco de Lucas, Effect of laser shock peening on the high temperature oxidation resistance of titanium, *Surface and Coatings Technology* 326 (2017) 146–155.
- [13] K. Chaudhuri, J. Perepezko, Microstructural study of the titanium alloy Ti-15Mo-2.7Nb-3Al-0.2Si (TIMETAL 21S), *Metallurgical and Materials Transactions A* 25 (1994) 1109–1118.

- [14] I. Polmear, D. StJohn, J.-F. Nie, M. Qian, 7 - titanium alloys, in: I. Polmear, D. StJohn, J.-F. Nie, M. Qian (Eds.), *Light Alloys (Fifth Edition)*, fifth edition ed., Butterworth-Heinemann, Boston, 2017, pp. 369 – 460.
- [15] K. K. Sankaran, R. S. Mishra, Chapter 5 - titanium alloys, in: K. K. Sankaran, R. S. Mishra (Eds.), *Metallurgy and Design of Alloys with Hierarchical Microstructures*, Elsevier, 2017, pp. 177 – 288.
- [16] A. Behera, S. Nag, K. Mahdak, H. Mohseni, J. Tiley, R. Banerjee, Influence of oxygen ingress on fine scale precipitation of  $\alpha$ -Ti during oxidation of Beta21S  $\beta$ -Ti alloy, *Journal of Materials Science* 48 (2013) 6700–6706.
- [17] C. Li, G. Li, Y. Yang, M. Varlioglu, K. Yang, Martensitic twinning in Alpha + Beta Ti-3.5Al-4.5Mo Titanium Alloy, *Journal of Metallurgy* 2011 (2011) 1–5.
- [18] Y. Mantani, Y. Takemoto, M. Hida, A. Sakakibara, M. Tajima, Phase transformation of  $\alpha'$  martensite structure by aging in Ti-8 mass%Mo Alloy, *Materials Transactions* 45 (2004) 1629–1634.
- [19] S. Guo, Q. Meng, X. Zhao, Q. Wei, H. Xu, Design and fabrication of a metastable  $\beta$ -type titanium alloy with ultralow elastic modulus and high strength, *Scientific Reports* 5 (2015) 14688.
- [20] D. Pionnier, M. Humbert, M. Philippe, Y. Combres, Study of the  $\alpha''$  phase texture obtained by martensitic  $\beta - \alpha''$  phase transformation induced by tensile test in a sheet of Ti5Al2Sn4Zr4Mo2Cr1Fe, *Acta Materialia* 46 (1998) 5891–5898.
- [21] M. C. Biesinger, L. W. M. Lau, A. R. Gerson, R. S. C. Smart, Resolving surface chemical states in XPS analysis of first row transition metals, oxides and hydroxides: Sc, Ti, V, Cu and Zn, *Applied Surface Science* 257 (2010) 887–898.
- [22] M. R. Alexander, G. E. Thompson, G. Beamson, Resolving surface chemical states in XPS analysis of first row transition metals, oxides and hydroxides: Sc, Ti, V, Cu and Zn, *Surface and Interface Analysis* 257 (2000) 468–477.
- [23] J. F. Moulder, W. F. Stickle, P. E. Sobol, K. D. Bomben, J. Chastein, R. K. Jr., *Handbook of X-Ray Photoelectron Spectroscopy*, Physical Electronics, Eden Prairie, 1995.
- [24] D. Monceau, B. Pieraggi, Determination of parabolic rate constants from a local analysis of mass-gain curves, *Oxidation of Metals* 50 (1998) 477–493.
- [25] P. Kofstad, High temperature corrosion, in *Physical Electronics*, Applied Science Publishers Ltd., London – New York, 1988 (1988).

- [26] T. A. Wallace, R. K. Clark, K. E. Wiedemann, Oxidation characteristics of Beta21S in air in the temperature range 600-800 °C, NASA Technical memorandum 104217 (1992), Hampton, VA (United States), Langley Res. Center (1992).
- [27] J. Stringer, G. Metcalf, M. Nicholson, The high-temperature oxidation of a commercial titanium-molybdenum alloy, *Journal of the Less Common Metals* 4 (1962) 69–77.
- [28] P. E. Blackburn, M. Hoch, H. L. Johnston, The vaporization of molybdenum and tungsten oxides, *The Journal of Physical Chemistry* 62 (1958) 769–773.
- [29] P. Trouslard, Pyrole: un logiciel au service des analyses par faisceau d'ions, Rapport CEA-R5703, 1995.
- [30] A. Zafari, K. Xia, Stress induced martensitic transformation in metastable  $\beta$  Ti-5Al-5Mo-5V-3Cr alloy: Triggering stress and interaction with deformation bands, *Materials Science and Engineering: A* 724 (2018) 75 – 79.
- [31] T. Grosdidier, C. Roubaud, M.-J. Philippe, Y. Combres, The deformation mechanisms in the  $\beta$ -metastable  $\beta$ -Cez titanium alloy, *Scripta Materialia* 36 (1997) 21 – 28.
- [32] X. Jiang, H. Zhao, R. Han, X. Zhang, M. Ma, R. Liu, Grain refinement and tensile properties of a metastable TiZrAl alloy fabricated by stress-induced martensite and its reverse transformation, *Materials Science and Engineering: A* 722 (2018) 8 – 13.

# High temperature oxidation resistance and microstructure of laser-shock peened Ti-Beta-21S

L. Lavisse<sup>a,\*</sup>, A. Kanjer<sup>a</sup>, P. Berger<sup>b</sup>, V. Optasanu<sup>a</sup>, C. Gorny<sup>c</sup>, P. Peyre<sup>c</sup>, T. Montesin<sup>a</sup>, M. C. Marco de Lucas<sup>a,\*</sup>

<sup>a</sup>*Laboratoire Interdisciplinaire Carnot de Bourgogne, UMR 6303 CNRS-Université Bourgogne-Franche Comté, 9 Avenue A. Savary, BP 47 870, F-21078 Dijon Cedex, France*

<sup>b</sup>*Université Paris-Saclay, CEA, CNRS, NIMBE, 91191 Gif-sur-Yvette, France*

<sup>c</sup>*Laboratoire PIMM - Ensam CNRS Cnam - Arts et Métiers - Sciences et Technologies - Ensam, 151 Bd de l'Hôpital, 75013 Paris France*

---

---

## Supplementary Material

### 1. Ion Beam Analysis techniques

Several Ion Beam Analysis techniques were used in this work. Figure S1 summarizes the operating principle of these techniques.

### 2. Hardness profiles

Micro-hardness profiles along the cross section of each sample were obtained using a ZWICK/ROELL ZHV $\mu$  microhardness tester with a Vickers diamond pyramid indenter and a load of 0.5 N on samples after mechanical treatments. The load was maintained for 10 s.

The hardness profiles along the thickness were measured on the cross-section of samples before and after LSP treatment. The results are given in Figure S2. The variation of the hardness value along the thickness was negligible of both kinds of samples, and the mean value was around 330 HV. The absence of strain hardening leads to the conclusion that the LSP treatment does not induce plastic deformation.

### 3. XPS

In order to investigate the chemical composition at the extreme surface, US and LSP samples were analysed by XPS before oxidation experiments at high temperature. Figure S3 shows the results obtained for untreated (US) and LSP

---

\*Corresponding authors

*Email addresses:* luc.lavisse@u-bourgogne.fr (L. Lavisse), delucas@u-bourgogne.fr (M. C. Marco de Lucas)

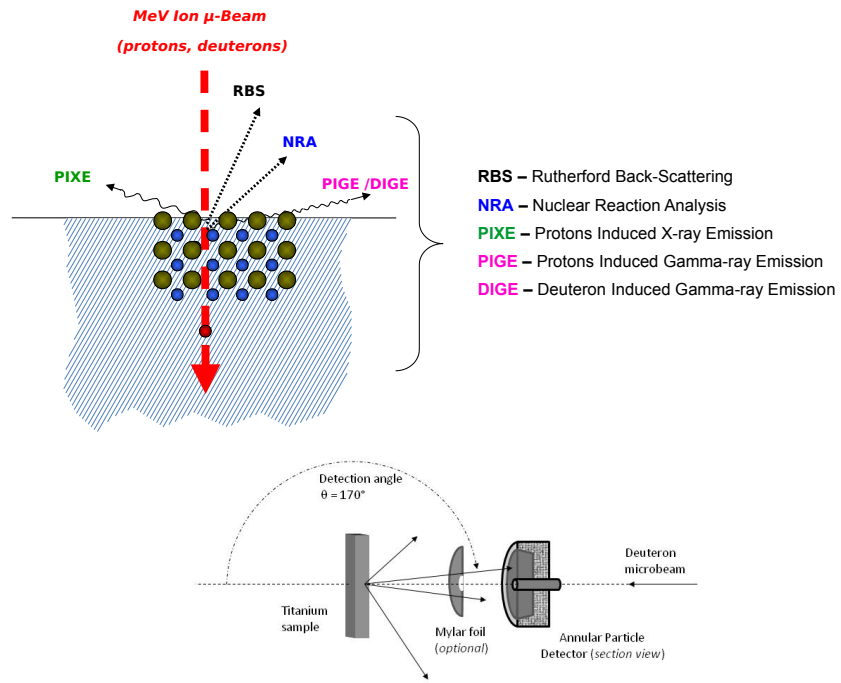


Figure S1: Operating principle of the different Ion Beam Analysis techniques used in this work, and sketch of the experimental setup.

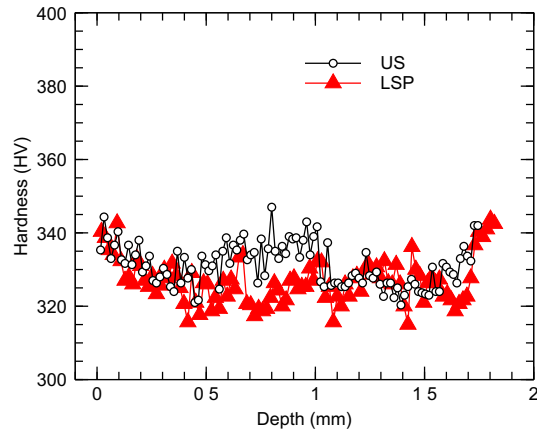


Figure S2: Hardness profiles measured on the cross-section of Ti-Beta-21S untreated (US) and LSP treated samples.

treated samples in the spectral ranges corresponding to the following XPS lines: Ti2p, Al2p, O1s, Mo3d, Mo3p and Nb3d.

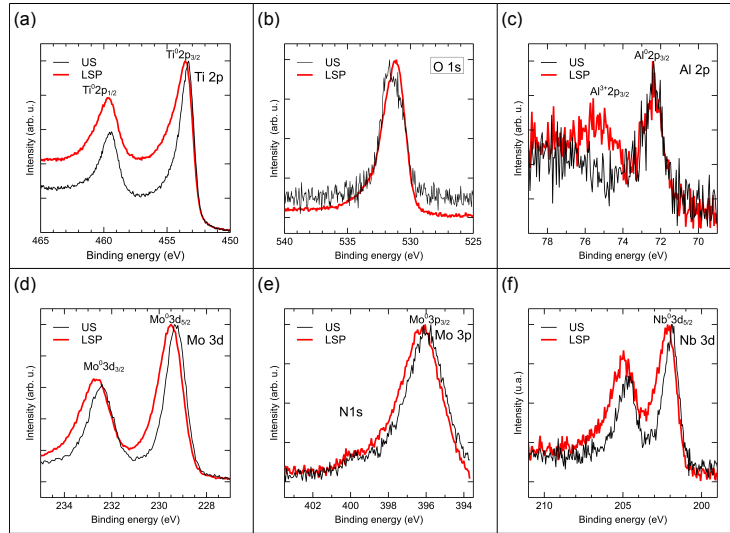


Figure S3: XPS spectra of untreated (US) and laser treated samples (LSP) in the spectral ranges corresponding to the following XPS lines: (a) Ti2p, (b) O1s and (c) Al2p, (d) Mo3d, (e) Mo3p, and (f) Nb3d.

#### 4. In-depth elemental concentration profiles of oxidized samples measured by EDS

Figure S4 shows the variation in depth of the atomic concentration of different elements (Ti, Al, Mo, O, N) in the cross-section of US and LSP samples after oxidation during 3000 h at 700 °C. The elemental concentrations were measured by using the EDS probe coupled to the SEM microscope.

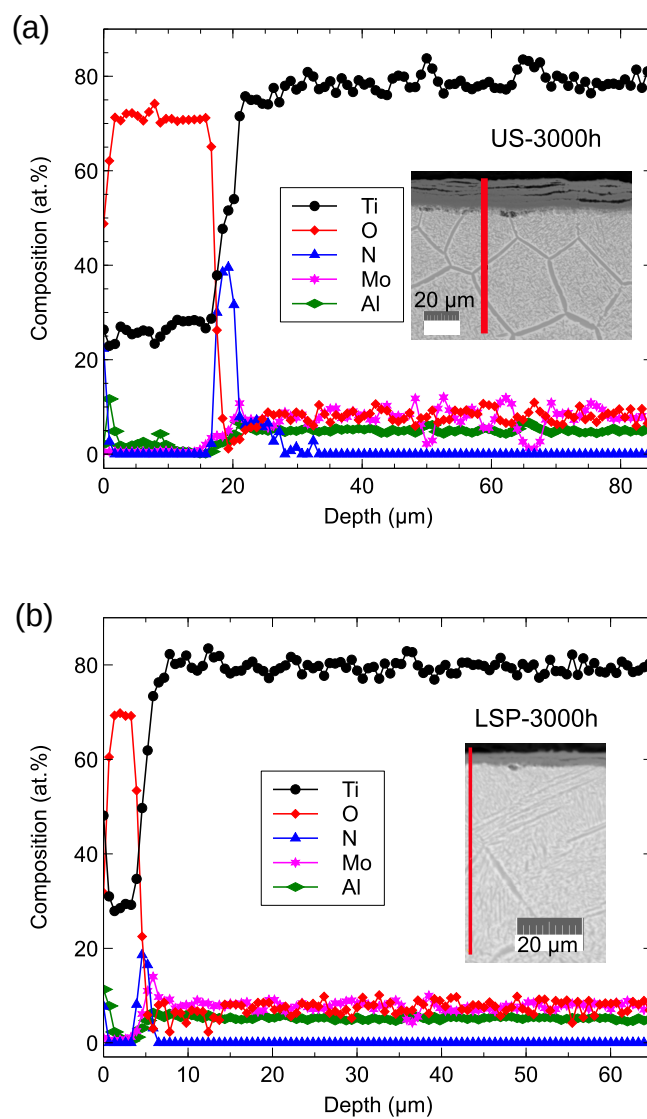


Figure S4: Variation in-depth of the atomic concentration of different elements (Ti, Al, Mo, O, N) measured by EDS in the cross-section of US and LSP samples after oxidation during 3000 h at 700 °C.

## 5. Profile in-depth of oxygen concentration by IBA experiments

The spatial distribution of oxygen in the cross section of oxidized samples was studied by IBA experiments. Deuteron Induced Gamma-Ray Emission (DIGE) spectra were recorded with a 1.9 MeV deuteron beam (spot size: 4.5  $\mu\text{m}$  x 3.5  $\mu\text{m}$ ). The surface was scanned over 200 x 200  $\mu\text{m}$ .

The maps of the spatial distribution of the DIGE signal assigned to oxygen for US-3000h and LSP-3000h samples (Figure 9) were used to extract the variation in-depth of the DIGE signal of oxygen (Figure 10).

The intensity of the oxygen signal was summed at each depth,  $X$ , in a 40  $\mu\text{m}$  large rectangle (red delimited domains in Figure 10) to increase the S/N ratio, and plotted as a function of depth ( $X$ ).

The atomic concentration of oxygen as a function of the depth was obtained as follows:

1. It was assumed that a native oxidation layer of titanium dioxide covers the whole surface of the sample cross-section. The DIGE signal of this native oxide layer together with the dark background signal were assumed to be the main contributions to the signal measured for the LSP-3000h at the deepest distance from the oxidation layer. So, it was subtracted from the experimental intensity of the oxygen signal all over the DIGE oxygen maps.
2. The difference in the slowing of the incident beam of deuterons as a function of the  $\text{TiO}_x$  stoichiometry was addressed by using the Pyrole software. The concentration of oxygen atoms ( $\text{atoms}/\text{cm}^2$ ) concerned by the analysis with the experimental conditions of this work was calculated for several  $\text{TiO}_x$  stoichiometries ( $x=2$  to  $0.01$ ). The results were fitted by a polynomial equation.
3. The DIGE signal of oxygen in the oxide scale of the sample US-3000h was assumed to correspond to  $\text{TiO}_2$ . The correspondence between the experimental DIGE signal of oxygen and the number of oxygen atoms per  $\text{cm}^2$  was calculated. Then, the corresponding stoichiometry was determined by using the polynomial equation previously obtained. The results are given in Figure S5.

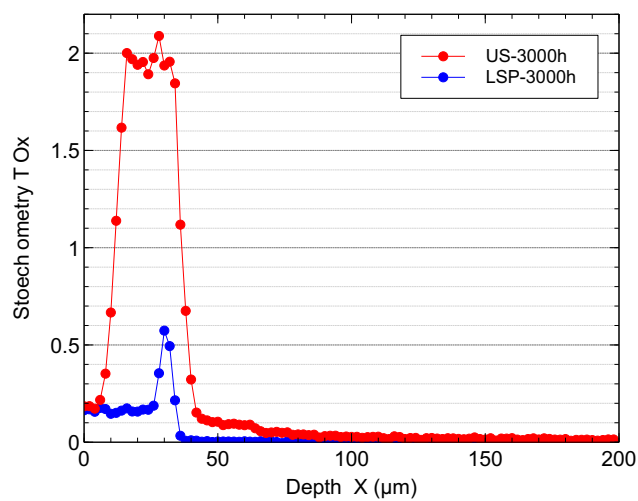


Figure S5: Stoichiometry as a function of the depth obtained from the cartography of the DIGE oxygen signal measured in the cross-section of US-3000h and LSP-3000h.